APPLIED SCIENCES AND ENGINEERING

Avalanches and power law behavior in aortic dissection propagation

Xunjie Yu[1], Béla Suki[2], Yanhang Zhang[1,2,3]*

Aortic dissection is a devastating cardiovascular disease known for its rapid propagation and high morbidity and mortality. The mechanisms underlying the propagation of aortic dissection are not well understood. Our study reports the discovery of avalanche-like failure of the aorta during dissection propagation that results from the local buildup of strain energy followed by a cascade failure of inhomogeneously distributed interlamellar collagen fibers. An innovative computational model was developed that successfully describes the failure mechanics of dissection propagation. Our study provides the first quantitative agreement between experiment and model prediction of the dissection propagation within the complex extracellular matrix (ECM). Our results may lead to the possibility of predicting such catastrophic events based on microscopic features of the ECM.

INTRODUCTION

Arterial dissection is a catastrophic event that may occur spontaneously or as a result of traumatic injuries in many arterial branches, including the aorta (*1*). It is characterized by the tearing of the intimal layer, which allows blood to enter between the lamellar layers of the aortic wall, resulting in the separation of the layers. A false lumen is formed in the separated media, which may narrow or occlude the true lumen. Because of diagnostic challenges, initial presentation of aortic dissection is missed in >30% of the cases (*2*). In the absence of intervention, acute aortic dissections result in mortality up to 90%, with most deaths occurring within 48 hours of the onset of aortic dissection (*3*). Thus, acute aortic dissection is one of the most devastating cardiovascular diseases. Once initiated, the dissection propagates rapidly, leading to high morbidity and mortality. The mechanisms underlying the propagation of aortic dissection, however, remain to be understood.

Prior studies of the biomechanics of aortic dissections, both experimental and computational, focused on the blood pressure and energy required for the propagation of an existing dissection (*4*, *5*). However, little is known about how aortic dissections propagate within the arterial wall, a highly inhomogeneous biological material. As an acute cardiovascular disease, aortic dissection is often associated with its rapid development, which presents substantial challenges in diagnosis and treatment. The sudden catastrophic nature of aortic dissections is largely unknown but may be similar to an avalanching behavior. Avalanches are events that are accompanied by a sudden transfer of energy or material with a wide range of magnitudes without a characteristic length scale (*6*). Avalanche behaviors have been found ubiquitously in nature, from sand piles (*7*), earthquakes (*8*), forest fires (*9*), neuronal assemblies (*10*), ciliary import (*6*), lung inflation (*11*), to cell microrheology (*12*). In an avalanching system, the energy or material accumulates gradually, driving the system to an unstable state. When a critical threshold is reached, the energy is released through avalanches of all sizes until the system returns back to a more stable state (*13*). Avalanching behavior is characterized by a power law distribution of avalanche sizes, exhibiting self-similar behavior over a wide range of scales. In this study, we hypothesized that aortic dissection propagates in an avalanche-like manner involving cascade failures of structural units within the arterial wall.

Understanding arterial dissection requires an understanding of the structure of the arterial wall. The extracellular matrix (ECM) in the arterial wall, composed of elastic fibers, collagen fibers, and ground substances including glycosaminoglycans/proteoglycans (GAGs/PGs), largely determines the passive mechanical properties of the artery. In the aortic media layer, these ECM components, together with smooth muscle cells, are organized into lamellar units, which are considered as the functional units of the artery (*14*). The concentric layers of elastic lamellae are interconnected through interlamellar elastic and collagen fibers and smooth muscle cells (*5*). However, the elastic and collagen fibers are distributed predominantly parallel to the lamellar planes, with minor amounts of interlamellar fibers. Because of the laminated structure of the aortic media, a tearing of the intima may propagate parallel to the lumen, forcing the layers apart (*15*). To study the possibility of avalanches in aortic dissection, we used the peeling test since it is more suited to quantify the fracture energy of the tissue (*5*). To this end, our study provides the first understanding of the mechanisms that govern the rapid propagation of aortic dissections.

RESULTS

To test our hypothesis that aortic dissection is due to avalanche-like cascade failures, we subjected aorta media samples to a slow peeling test that allowed us to mimic the propagation of aortic dissection. The peeling force F (normalized by the width of the sample) showed notable fluctuations for both circumferential (Fig. 1A) and longitudinal samples (Fig. 1B). The mean force in the longitudinal direction was statistically significantly higher ($P = 0.0138$) than that in the circumferential direction (fig. S1A and table S1), indicating anisotropic dissection properties of aortic media. Consistently, the dissection energy W^{dissect} in the longitudinal direction tended to be higher ($P = 0.0611$) than that in the circumferential direction (fig. S1B and table S1).

In all samples studied, the force traces during dissection propagation were composed of a sharp initial increase, a jagged plateau region, and a sudden drop, marking the full separation of the sample (Fig. 1C). The plateau region displayed many sudden force drops of

[1]Department of Mechanical Engineering, Boston University, Boston, MA 02215, USA. [2]Department of Biomedical Engineering, Boston University, Boston, MA 02215, USA. [3]Divison of Materials Science & Engineering, Boston University, Boston, MA 02215, USA. *Corresponding author. Email: yanhang@bu.edu

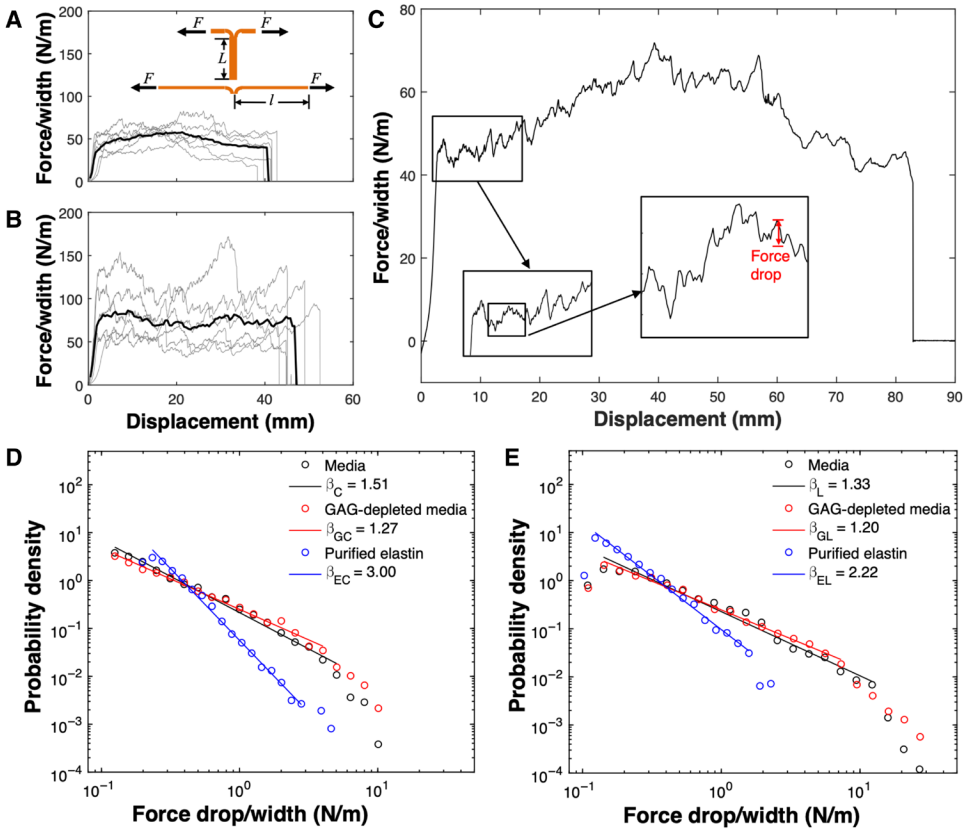

Fig. 1. Power law behavior in dissection propagation within the aortic media. Peeling force (force per unit width) versus displacement for (**A**) circumferentially oriented aortic media and (**B**) longitudinally oriented aortic media ($n = 6$). The thick curve characterizes the arithmetic mean response. Inset figure shows schematic drawings of the peeling test experimental setup before loading and right before full separation. *L* is the effective length of the tissue, and *l* is the length of the tissue right before separation. (**C**) Representative peeling force (force per unit width) versus displacement curve showing the fluctuating force profile during peeling test. Force drop was calculated as the difference between the peak and following valley. Probability density distribution of the force drops in dissection propagation within the media, GAG-depleted media, and purified elastin samples in (**D**) the circumferentially oriented samples, and (**E**) the longitudinally oriented samples. Straight lines in (D) and (E) represent linear fits to the experimental data in double logarithmical graphs, and β is defined as the negative slope of a straight line fit. Here, subscripts C, GC, and EC represent the media, GAG-depleted media, and purified elastin, respectively, in the circumferential direction; subscripts L, GL, and EL represent the media, GAG-depleted media, and purified elastin, respectively, in the longitudinal direction.

various magnitudes. The size distribution of these force drops was calculated and presented in double logarithmical graphs in Fig. 1 (D and E). The resulting probability density distribution of force drops showed a linear decrease implying a power law distribution over almost two orders of magnitude from 0.1 to 10 N/m. The power law distribution in the circumferential and longitudinal direction had an exponent β, defined as the negative slope of a straight line fit, of 1.51 and 1.33 ($P < 0.05$), respectively (Fig. 1, D and E). The power law behavior implies that the force drops have no characteristic scale, and hence, the dissection process is not dominated by any specific length scale other than the system size, which is consistent with the force drops originating from avalanche failures of the material in the arterial wall. While the avalanche size is determined by the force drops, the avalanche duration is related to the displacement increment between two consecutive force drops. The dissection energy can be approximated by computing the triangular area enclosed by the avalanche size (force drop) and the displacement increment by which the avalanche advances. The probability density distributions of the displacement increments and dissection energy also follow a power law (fig. S2).

To investigate the microscopic structural origins of failures, multiphoton images were taken at the separation point (Fig. 2, A and B), which showed interlamellar elastic and collagen fibers connecting the two elastic lamellar layers being separated. Compared with the dense elastic and collagen fibers that form the lamellar layers, interlamellar fibers are more sparsely arranged, and their distributions are highly nonuniform in density and orientation (Fig. 2, C and D). This suggests that the local interlamellar resistance to layer separation could vary markedly during the peeling process. From the side view, the cross section of two adjacent lamellar units being separated formed the V shape of the dissection front (Fig. 2, E and F). The elastic lamellae are bent because of the pulling from the interlamellar collagen and elastin fibers. In circumferential dissection, only two adjacent layers can be seen to be involved, indicating that the dissection propagates mainly between the two adjacent layers (Fig. 2, A, C, and E). In longitudinal dissection, however, multiple lamellar units are involved (Fig. 2, B, D, and F), suggesting that the dissection may separate several lamellar layers during its propagation. This is another evidence of the anisotropic dissection property of the arterial wall apart from the different peeling forces in the circumferential and longitudinal directions.

To understand the contribution of ECM components to the power law behavior and the associated avalanches, the force drops were

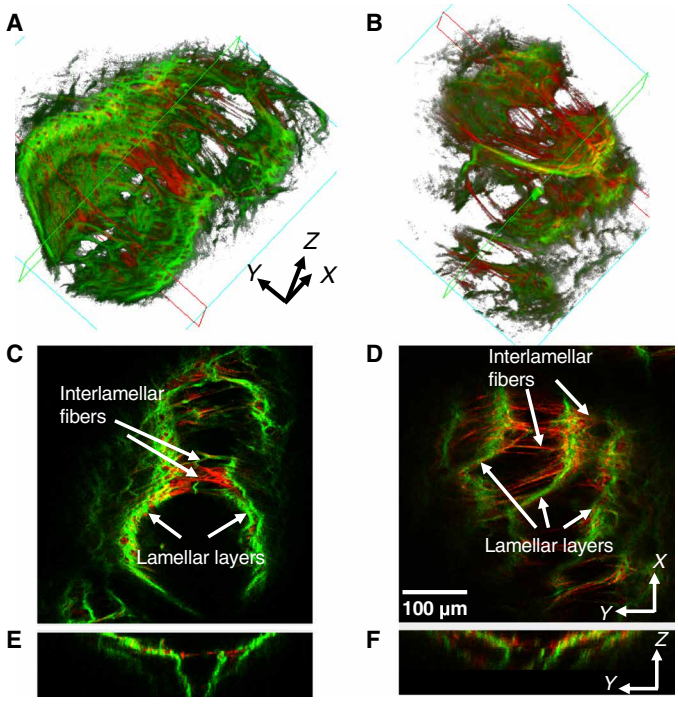

Fig. 2. Multiphoton images of dissected aortic media at the dissection front. Three-dimensional reconstructed images of (**A**) circumferentially oriented and (**B**) longitudinally oriented dissected sample. Two-dimensional view in the *xy*- and *yz*-planes for (**C** and **E**) a circumferentially oriented sample, in which two adjacent lamellar layers are being separated, and (**D** and **F**) a longitudinally oriented sample, in which multiple lamellar layers are involved. Collagen fibers are shown in red and elastic fibers in green. Interlamellar fibers can be seen connecting the two lamellar layers that are being separated.

calculated from the peeling test of GAG-depleted media and purified elastin (Fig. 1, D and E). GAG depletion leads to similar dissection behavior as the control media (fig. S3, C and D) albeit with higher dissection force and energy (fig. S1, A and B) and an increase in dissection energy in the circumferential direction being significant ($P = 0.0478$). Although the power law behavior remained in the GAG-depleted media, there was a slight decrease in the power law exponents to 1.27 ($P = 0.0004$) and 1.20 ($P = 0.024$) in the circumferential and longitudinal direction, respectively. This suggests that the mechanism of failure is related to other components of the arterial wall such as collagen and/or elastin. Further experiments with purified elastin network, in which both collagen and GAGs were removed, resulted in significant decreases in both dissection force and energy ($P < 0.0001$; fig. S3, A and B, and table S1). The power law exponents increased to 3.00 in the circumferential direction and 2.22 in the longitudinal direction, both of which were significantly higher ($P < 0.0001$) than those of the intact aortic media (Fig. 1, D and E). The drastic increase in the exponents and the associated reduced sizes in the avalanches provide evidence that the interlamellar collagen fibers play a dominant role in maintaining the integrity of the arterial wall.

To further determine the mechanism that governs the dissection process, a finite element model capturing the dissection propagation in the peeling test was created that included discrete interlamellar connecting fibers with material properties similar to those of collagen fibers (Fig. 3A). During layer separation, avalanches were generated when interlamellar fibers were gradually stretched until failure. The V shape of the dissection front was also captured by the model (Fig. 3B). The force displacement curve in the longitudinal direction was higher than that in the circumferential direction, indicating higher separation force (Fig. 3C), which is in accord with the observations from the controlled peeling test (fig. S1A). The corresponding distribution of the force drops from the model is also consistent with a power law in both circumferential and longitudinal directions, with exponents of 1.52 and 1.34, respectively (Fig. 3D). These exponents agree very well with those from the experiments [1.51 and 1.33 in the circumferential and longitudinal directions, respectively, as shown in Fig. 1 (D and E)]. When elastic fibers were introduced into the model, the power law distribution remained roughly the same (fig. S4).

Both structural and mechanical inhomogeneities were introduced into the finite element model through considering the randomness in fiber density, orientation, and strain at failure. The model successfully captured the avalanche behavior during the propagation of aortic dissection (Fig. 3D). To pinpoint the origin of the power law behavior and exponents, mechanical and structural inhomogeneities were selectively eliminated from the model. When mechanical inhomogeneity was eliminated from the model by assuming uniform fiber failure strain for all interlamellar collagen fibers, the power law distribution of force drops maintained the same exponent of 1.51 (Fig. 4A). However, when structural inhomogeneity was eliminated by having evenly spaced parallel interlamellar fibers between the adjacent elastic lamellae, the power law behavior completely disappeared (Fig. 4A), indicating that structural inhomogeneity is the ultimate source of the power law behavior in delaminating the lamellar layers.

The model also reveals an interesting interplay between the mechanical properties of interlamellar fibers and the lamellar layers in the propagation of lamellar layer separations. When the shear modulus of the bulk tissue was increased from 180 to 360 kPa, the power law distribution of force drops remained, but the exponent increased with shear modulus, from 1.18 to 1.67 (Fig. 4B). When the mean strain at failure increased from 0.05 to 0.30, the exponent showed a decreasing trend, mainly between failure strains of 0.1 and 0.25 (Fig. 4C).

DISCUSSION

Acute aortic dissection occurs within 2 weeks of onset with approximately 65 to 75% death rate without treatment (*16*). In particular, aortic dissections are so catastrophic that about 20% of patients die before reaching a hospital (*17*). In DeBakey's classification, type I aortic dissection, which is the most frequent aortic dissections (accounting for about 60 to 70% of incidence) and is of higher risk, originates in the ascending thoracic aorta and often quickly advances through the entire aorta (*18*, *19*). In this study, we found that the dissection propagates in avalanches. An important characteristic of an avalanching system is the broad distribution of the event sizes that results from a gradual buildup of stress at the front of the dissection followed by a sudden rupture and energy release via an avalanche. In aortic dissection, avalanches can produce force drops with magnitudes spanning over almost two decades, which break the interlamellar bonding and advance the front of dissection through the adjacent layers of lamellar units. This may provide an explanation for the rapid propagation of the aortic dissection throughout the entire aorta. Avalanche behavior has been reported for other materials with

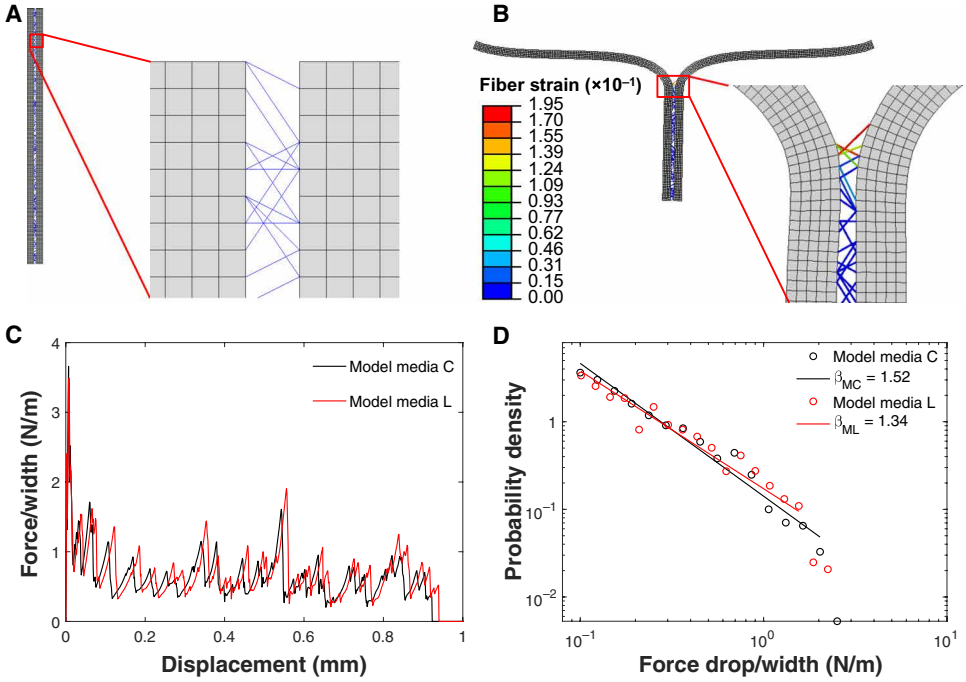

Fig. 3. Power law behavior of dissection propagation simulated using a finite element model considering the discrete interlamellar collagen fibers. (**A**) Finite element model showing the two media strips connected via discrete interlamellar collagen fibers. (**B**) Engineering strain in the interlamellar fibers during dissection propagation. Fibers that reached failure criteria were automatically removed from the model. It can be seen that the fibers exactly at the front of the separation are the most stretched. (**C**) Peeling force (force per unit width) versus displacement from the finite element simulation. (**D**) Probability density distribution of the force drops in dissection propagation within the aortic media from simulations. Straight lines represent linear fits to the model results in double logarithmical graphs, and β is defined as the negative slope of a straight line fit. Here, subscripts MC and ML represent the model results in the circumferential and longitudinal directions, respectively.

fibrous microstructure, such as wood, fiber glass, and paper, with unique exponents that characterize the probability of microfractures (*20*–*22*). However, to our knowledge, this is the first study to report fracture-related avalanches in a biological material.

The adjacent elastic lamellar layers are connected by interlamellar elastic and collagen fibers (Fig. 2), which are the key elastic elements contributing to the force development during lamellar separation. The interlamellar fibers also play an important role in transferring the transmural stress across the wall (*23*). In the force displacement curve, the fluctuating force profile of individual samples in Fig. 1C originates from the failure of nonuniformly distributed interlamellar fibers. Each force drop corresponds to one small avalanche or microfailure that may be composed of multiple fibers rupturing simultaneously. From the estimation of interlamellar fiber strength, it is unlikely that a single microfailure corresponds to the failure of an individual interlamellar fiber (*24*). Rather, the microfailure is likely due to a group of inhomogeneously arranged interlamellar collagen fibers rupturing in a single avalanche. When dissection advances between the lamellar layers, the interlamellar fibers are stretched and store more elastic energy. Consequently, stress concentration gradually builds up at the front of the dissection. When the strain in an interlamellar fiber reaches its failure limit, the fiber fails, and the load it carried before rupture is redistributed among the neighboring intact fibers. Since the failure threshold of the fibers is similar, failure of a single fiber can immediately stretch more fibers beyond their failure threshold. Consequently, these neighboring fibers will also fail in a rapid succession, generating an avalanche.

The exponents of the power law distribution of the force drops during lamellar dissection are within the range of avalanche behavior in the model of self-organized criticality (*25*). Systems with the ability to self-organize to criticality have a potential for extreme behavior, which, in our study, would be the avalanche-like macroscopic layer separation in the arterial wall. Several computational models have been proposed to study the power law behavior (*25*–*28*). However, computational models are often oversimplified, and their exponents may not match those found in experimental studies (*20*). In this study, to simulate the peeling process and recapitulate the power law distribution, we created a finite element model that considers the contribution of discrete interlamellar collagen fibers. The particular composition of the interlamellar fibers in the model was based on our experimental data from GAG-depleted and purified elastin samples, suggesting that, by far, the contribution of collagen dominates the avalanche behavior (Fig. 1, D and E). A previous study also showed no significant difference in dissection energy when elastin was removed from the media (*29*). The inhomogeneity of the interlamellar fibers was included by introducing the randomness in the interlamellar fiber orientation and density, as well as the failure strain. Compared with earlier statistical models of parallel fiber bundles (*26*), this inhomogeneity was introduced along the propagation direction of the dissection. The model simulated the controlled peeling process in the experiment by separating the media from the interlamellar space (Fig. 3, A and B). When the dissection propagates through the region where the interlamellar fibers are distributed sparsely, the fibers break, generating discrete force drops (Fig. 1C). The resistance against the advance of a crack in the material gradually builds up when the

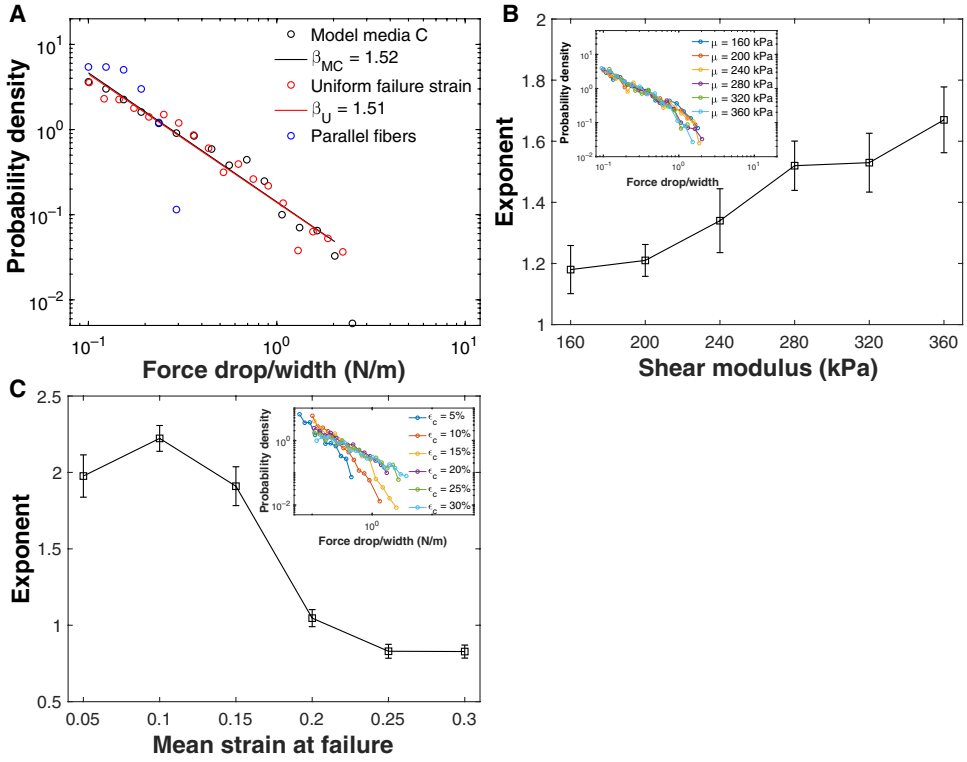

Fig. 4. Effects of structural and material properties on the power law behavior. (**A**) Effects of structural and mechanical inhomogeneity on the power law behavior. The structural inhomogeneity in fiber orientation and density was removed by having equally spaced parallel interlamellar collagen fibers, in which case the power law behavior completely disappeared. The mechanical inhomogeneity was removed by letting all interlamellar fibers have the same failure strain. The power law behavior remained, and the exponent was not substantially different. Straight lines represent linear fits to the model results in double logarithmical graphs, and β is defined as the negative slope of a straight line fit. Here, subscript MC represents the model results in the circumferential direction, same as in Fig. 3D, and subscript U represents the model results when all interlamellar fibers have the same failure strain. (**B**) Effect of shear modulus of the medial layer on the power law behavior. Exponents from the model results were plotted versus the shear modulus of the media in the model. The inset figure shows the probability density distribution of the force drop/width. (**C**) Effect of mean failure strain of interlamellar collagen fibers on the power law behavior. The inset figure shows the probability density distribution of the force drop/width. Error bars represent SEM.

dissection front reaches a region where the interlamellar fibers are more densely distributed. Moreover, the angled interlamellar fibers can reorient and stretch during the separation before the deformation exceeds their failure strain (Fig. 3B), which increases the force required to propagate the dissection. When the fibers at the dissection front fail, the dissection advances easily through the neighboring scattered fibers, creating successive avalanches.

ECM fibers in the arterial wall are structurally and mechanically inhomogeneous. Both mechanical and structural inhomogeneities were found to control the peeling strength and the resistance to delamination (*30*, *31*). In our model, the mechanical inhomogeneity is reflected in the random failure strain of interlamellar fibers. The variance of failure strain of elastic and collagen fibers have been observed in tensile tests of a single fiber (*32*, *24*). Our study (Fig. 4A), along with others (*26*), showed that the power law distribution does not depend on the mechanical inhomogeneity. The structural inhomogeneity is present as a nonuniform spatial distribution of interlamellar fibers, in terms of the fiber density along the dissection direction, as well as their orientation with respect to lamellar layers. The structural inhomogeneity can be observed in multiphoton images at the dissection location during controlled peeling (Fig. 2). Our study showed that structural inhomogeneity is the underlying mechanism of the avalanche behavior in the propagation of aortic dissection (Fig. 4A). In other words, this random structural arrangement in interlamellar fibers is the source of the generated avalanches of energy release, or force drop, on a wide range of scales (Fig. 1, D and E).

The anisotropic mechanical properties of the arterial wall were considered through different shear moduli in the circumferential and longitudinal directions and resulted in slightly different power law exponents in the two directions (Fig. 3D). With stiffer tissue, the forefront of interlamellar fibers at the separation point were more likely to be fully engaged than fibers further away from the forefront and the fibers within the lamellar layers (Fig. 2, A and B). This then decreased the probability of higher force drops and resulted in smaller avalanches and a larger power law exponent (Fig. 4B). When the failure strain of fibers increased, however, more interlamellar fibers were engaged before failure. As a result, the probability of higher force drops increased, resulting in larger avalanches and a smaller power law exponent (Fig. 4C). Nevertheless, in both cases, the power law form of the distribution of the force drops was not affected.

The power law distribution of force drops is consistent in the aortic media and the GAG- depleted media samples, in both circumferential and longitudinal directions, although with slightly different exponents (Fig. 1, D and E). This suggests that the power law behavior is fundamentally associated with the structural organization of the aortic wall, regardless of the changes in its composition following GAG

depletion. Recent studies pointed out that local accumulation of GAGs/PGs could initiate aortic dissections by increasing the intralamellar swelling pressure and thus the intramural mechanical stress field (*33*, *34*). Consistent with these previous suggestions, our results showed an increasing trend in energy required to propagate the dissection after the removal of GAGs (fig. S1).

It is interesting to point out that in aortic media, the average peeling force in our experiments was about 50 N/m (Fig. 1A). According to the Law of Laplace, a physiological blood pressure of 100 mmHg results in a wall tension of about 130 N/m in a lumen with a radius of 1 cm, which is more than twice the peeling force. Thus, when blood enters and accumulates within the interlamellar space, the physiological blood pressure is high enough to propagate the lamellar layer separation. Also, although not fully understood at the moment, the pulsatile pressure in physiological conditions could potentially expedite the peeling process considering the complex interplay between the viscoelastic behavior of the arterial tissue and the intermittent stress relief and rapid buildup associated with the pulsatile pressure.

The current study is conducted in normal tissue. Future work is needed to understand the dissection behavior in diseased tissue. Furthermore, only interlamellar elastic and collagen fibers were considered in the model. It would be interesting to incorporate the effects of smooth muscle activation and the presence of GAG pools (*35*) and in-plane fiber failure on the separation of lamellar layers (*36*), especially in studying diseased tissue.

CONCLUSION

Our findings provide evidence that aortic dissections propagate via avalanches of various sizes that follow a power law distribution. The avalanche behavior results from the local buildup of strain energy followed by a cascade of mechanical failures, a key component of which is the inhomogeneous spatial distribution of interlamellar collagen fibers in the aortic media. Our study further suggests that the interlamellar fiber inhomogeneity governs the rapid evolution of aortic dissection by avalanches. Thus, characterizing the ECM structural inhomogeneity in vivo with future imaging modalities may provide a useful index of the risk of developing dissections.

MATERIALS AND METHODS

Sample preparation

Porcine descending thoracic aortas were harvested at 12 to 24 month of age at a local abattoir and transported to the laboratory on ice. After removing the adhesive tissue and fat, samples were cut into strips with dimensions of about 40 mm by 10 mm with the long edge parallel to either the longitudinal or the circumferential direction of the artery. A total of 36 samples were obtained from six aortas. Among these 36 samples, 18 were in the circumferential direction, and 18 were in the longitudinal direction. The samples in each direction were then divided into three groups with $n = 6$ for each group. The adventitia was carefully removed to ensure that either side of the tear will have similar mechanical properties.

The first sample group was kept as control and underwent no treatment. The second group was subjected to an enzymatic treatment to remove GAGs (*37*). Briefly, samples were treated in 100 mM ammonium acetate buffer [(pH 7.0), hyaluronidase (2 to 5 U/ml), chondroitinase ABC, (0.025 U/ml), and heparinase (0.25 U/ml); Sigma-Aldrich #H3506, C3667, and H3917, St. Louis, MO] and gently agitated for 24 hours at 37°C to remove GAGs. The third group was subjected to a cyanogen bromide treatment to obtained purified elastin in which collagen, GAGs, and smooth muscle cells were removed (*38*). Samples were then rinsed and kept in phosphate-buffered saline for further mechanical testing and multiphoton imaging.

Peeling test

A small incision was made at the center of the media to initiate a failure. The samples were split at the incision to get two tongues of about 10-mm long and approximately equal thickness. Sandpapers were glued to both sides of the tongues to prevent slippage between the sample and the clamps. The two tongues were then clamped to the uniaxial tensile tester (Instron 5800) for peeling tests. The distance from the separation point to the other end of the sample, the effective length L (see the inset Fig. 1A), was measured using a digital caliper and summarized for all samples in table S1. The peeling test was then performed with an extension rate of 0.2 mm/s (*39*), during which the force and displacement were recorded. The mean peeling force value of each sample was calculated as the arithmetic mean of the force values in the plateau region divided by the width of the sample. The computed mean peeling force values were then averaged within the experimental groups to obtain the mean peeling force for each group (fig. S1A).

Dissection energy

Dissection energy, i.e., the energy required to propagate the dissection, was used to quantify the peeling properties of the samples (*5*). During the peeling process, the total external work in both directions can be calculated as

$$W^{\text{ext}} = 2Fl$$

where F is the mean force per unit width, and l is the length of the tissue right before separation (Fig. 1A). The total work can be decomposed into two parts: the elastic stored energy and dissipated dissection energy. The dissection energy per reference area can then be determined as

$$W^{\text{dissect}} = (W^{\text{ext}} - W^{\text{elastic}})/L$$

where L is the effective length of tissue. By assuming a linear relationship between stress and strain, the elastic stored energy can be estimated as

$$W^{\text{elastic}} = F(l - L)$$

where $l - L$ is the change in tissue length. Additional details can be found from Sommer *et al.* (*5*).

Multiphoton imaging

A multiphoton microscopy system (Carl Zeiss LSM 710 NLO) with a 810-nm femtosecond infrared pulse laser excitation was used to generate two-photon excited fluorescence from elastin (525/45 nm) and second harmonic generation from collagen (417/80 nm) as in our previous study (*40*). The laser scanning system was coupled to an upright microscope with a 20× water immersion objective lens. A custom-built device was used so that the sample could be imaged at the dissection front during the peeling process. Samples

in circumferential and longitudinal directions were imaged with a field view of 425 μm × 425 μm to obtain an image stack of about 50 μm in depth. Three-dimensional images were generated using Volume Viewer plugin (developed by K. U. Barthel) in Fiji (http:/Fiji.sc/Fiji; Ashburn, VA).

Finite element modeling

A finite element model was created to simulate the dissection process in Abaqus 6.14. The model consisted of two pieces of lamellar layers (2-mm long, 5-μm wide, and 50-μm thick) with interconnecting collagen fibers. The element size for the lamellar layers is 0.01 mm. Neo-Hookean model was used to describe the mechanical behavior of the lamellar layers (*41*). Since the aortic media is stiffer in the circumferential than in the longitudinal direction, the shear modulus in the circumferential direction was set to be 280 kPa while that in the longitudinal direction was 240 kPa. The distance between the two pieces of media was 20 μm, which is a typical value for interlamellar distance (*42*). A set of 300 collagen fibers with a diameter of 1 μm were generated and randomly attached to the two pieces of media to mimic the spatial arrangement of interlamellar fibers between adjacent lamellar layers. The orientation of interlamellar fibers was randomly generated following a uniform distribution from −60° to 60° from the dissection plane. The collagen fibers were modeled with the following stress-strain relationship $\sigma = 5.4 \times [\mathrm{Exp}(5\varepsilon) - 1]$ MPa (*43*) where σ is the stress, and ε is the engineering strain. The strain at failure followed a uniform distribution from 0.107 to 0.207 based on the reported tensile strength (*24*). In another model, 100 interlamellar elastic fibers with 0.1 μm in diameter (*44*) were generated and added to the interlamellar space following the same procedure. The elastic fibers had linear elasticity with a stiffness of 0.8 MPa and a failure strain following a uniform distribution from 0.9 to 1.1 (*32*). The interlamellar fibers were modeled with Timoshenko (shear flexible) beam elements (B21H). To simulate the layer separation process in the controlled peeling test, the two ends of media were prescribed to move away from each other horizontally until the two sides of the media separated. The peeling force was computed as the sum of the reaction forces of all the nodes at the corresponding boundary. The shear modulus of the elastic lamellae, the mean failure strain, and the distribution of the interlamellar fibers were then varied to examine their effects on the power law behavior. The shear modulus of elastic lamella was varied from 160 to 360 kPa in 40-kPa increments. The mean failure strain of the interlamellar fibers was varied from 0.05 to 0.3 with 0.05 increment.

Statistical analysis

Peeling forces and dissection energy were presented as means ± SEM. The force per unit width and fracture energy in each experimental group were compared to the control group using Student unpaired *t* test. The power law exponents were obtained by fitting a straight line to each distribution on a log-log graph and compared by *t* tests, assuming that they were normally distributed and using the estimated variance from the linear regression. $P < 0.05$ is considered to be statistically significant.

SUPPLEMENTARY MATERIALS

Supplementary material for this article is available at http://advances.sciencemag.org/cgi/content/full/6/21/eaaz1173/DC1

View/request a protocol for this paper from *Bio-protocol*.

REFERENCES AND NOTES

1. T. C. Gasser, G. A. Holzapfel, Modeling the propagation of arterial dissection. *Eur. J. Mech. A/Solids* **25**, 617–633 (2006).
2. C. A. Nienaber, R. E. Clough, N. Sakalihasan, T. Suzuki, R. Gibbs, F. Mussa, M. P. Jenkins, M. M. Thompson, A. Evangelista, J. S. M. Yeh, N. Cheshire, U. Rosendahl, J. Pepper, Aortic dissection. *Nat. Rev. Dis. Primers* **2**, 16053 (2016).
3. N. T. Kouchoukos, D. Dougenis, Surgery of the thoracic aorta. *N. Engl. J. Med.* **336**, 1876–1889 (1997).
4. M. W. Carson, M. R. Roach, The strength of the aortic media and its role in the propagation of aortic dissection. *J. Biomech.* **23**, 579–588 (1990).
5. G. Sommer, T. C. Gasser, P. Regitnig, M. Auer, G. A. Holzapfel, Dissection properties of the human aortic media: An experimental study. *J. Biomech. Eng.* **130**, 021007 (2008).
6. W. B. Ludington, K. A. Wemmer, K. F. Lechtreck, G. B. Witman, W. F. Marshall, Avalanche-like behavior in ciliary import. *Proc. Natl. Acad. Sci. U.S.A.* **110**, 3925–3930 (2013).
7. H. M. Jaeger, S. R. Nagel, Physics of the granular state. *Science* **255**, 1523–1531 (1992).
8. A. Sornette, D. Sornette, Self-organized criticality and earthquakes. *Europhys Lett* **9**, 197–202 (1989).
9. B. D. Malamud, G. Morein, D. L. Turcotte, Forest fires: An example of self-organized critical behavior. *Science* **281**, 1840–1842 (1998).
10. J. M. Beggs, D. Plenz, Neuronal avalanches in neocortical circuits. *J. Neurosci.* **23**, 11167–11177 (2003).
11. B. Suki, A.-L. Barabási, Z. Hantos, F. Peták, H. E. Stanley, Avalanches and power-law behaviour in lung inflation. *Nature* **368**, 615–618 (1994).
12. B. Fabry, G. N. Maksym, J. P. Butler, M. Glogauer, D. Navajas, J. J. Fredberg, Scaling the microrheology of living cells. *Phys. Rev. Lett.* **87**, 148102 (2001).
13. M. Paczuski, S. Maslov, A. Per Bak, Avalanche dynamics in evolution, growth, and depinning models. *Phys Rev E* **53**, 414 (1996).
14. H. Wolinsky, S. Glagov, A lamellar unit of aortic medial structure and function in mammals. *Circ. Res.* **20**, 99–111 (1967).
15. A. S. Tam, M. Catherine Sapp, M. R. Roach, The effect of tear depth on the propagation of aortic dissections in isolated porcine thoracic aorta. *J. Biomech.* **31**, 673–676 (1998).
16. R. W. DeSanctis, R. M. Doroghazi, W. G. Austen, M. J. Buckley, Aortic dissection. *N. Engl. J. Med.* **317**, 1060–1067 (1987).
17. J. Golledge, K. A. Eagle, Acute aortic dissection. *Lancet* **372**, 55–66 (2008).
18. C. E. Anagnostopoulos, M. J. Prabhakar, C. F. Kittle, Aortic dissections and dissecting Aneurysms. *Am. J. Cardiol.* **30**, 263–273 (1972).
19. M. E. DeBakey, C. H. McCollum, E. S. Crawford, G. C. Morris Jr., J. Howell, G. P. Noon, G. Lawrie, Dissection and dissecting aneurysms of the aorta: Twenty-year follow-up of five hundred twenty-seven patients treated surgically. *Surgery* **92**, 1118–1134 (1982).
20. A. Guarino, A. Garcimartín, S. Ciliberto, An experimental test of the critical behaviour of fracture precursors. *Eur. Phys. J. B.* **6**, 13–24 (1998).
21. L. I. Salminen, A. I. Tolvanen, M. J. Alava, Acoustic emission from paper fracture. *Phys. Rev. Lett.* **89**, 185503 (2002).
22. C. Maes, A. Van Moffaert, H. Frederix, H. Strauven, Criticality in creep experiments on cellular glass. *Phys. Rev. B* **57**, 4987 (1998).
23. J. E. Wagenseil, R. P. Mecham, Vascular extracellular matrix and arterial mechanics. *Physiol. Rev.* **89**, 957–989 (2009).
24. H. Miyazaki, K. Hayashi, Tensile tests of collagen fibers obtained fromt he rabbit patelar tendon. *Biomed. Microdevices* **2**, 151–157 (1999).
25. P. Bak, C. Tang, K. Wiesenfeld, Self-organized criticality: An explanation of the 1/ *f* noise. *Phys. Rev. Lett.* **59**, 381–384 (1987).
26. S. Pradhan, A. Hansen, B. K. Chakrabarti, Failure processes in elastic fiber bundles. *Rev. Mod. Phys.* **82**, 499–555 (2010).
27. L. De Arcangelis, S. Redner, H. J. Herrmann, A random fuse model for breaking processes. *J. Phys. Lettres* **46**, 585–590 (1985).
28. S. Zapperi, A. Vespignani, H. E. Stanley, Plasticity and avalanche behaviour in microfracturing phenomena. *Nature* **388**, 658–660 (1997).
29. C. Noble, N. Smulders, R. Lewis, M. J. Carré, S. E. Franklin, S. MacNeil, Z. A. Taylor, Controlled peel testing of a model tissue for diseased aorta. *J. Biomech.* **49**, 3667–3675 (2016).
30. A. Tsamis, J. A. Phillippi, R. G. Koch, S. Pasta, A. D'Amore, S. C. Watkins, W. R. Wagner, T. G. Gleason, D. A. Vorp, Fiber micro-architecture in the longitudinal-radial and circumferential-radial planes of ascending thoracic aortic aneurysm media. *J. Biomech.* **46**, 2787–2794 (2013).
31. S. Pal, A. Tsamis, S. Pasta, A. D'Amore, T. G. Gleason, D. A. Vorp, S. Maiti, A mechanistic model on the role of "radially-running" collagen fibers on dissection properties of human ascending thoracic aorta. *J. Biomech.* **47**, 981–988 (2014).
32. R. W. Carton, J. Dainauskas, J. W. Clark, Elastic properties of single elastic fibers. *J. Appl. Physiol.* **17**, 547–551 (1962).
33. J. D. Humphrey, Possible mechanical roles of glycosaminoglycans in thoracic aortic dissection and associations with dysregulated transforming growth factor-β. *J. Vasc. Res.* **50**, 1–10 (2012).

34. S. Roccabianca, G. A. Ateshian, J. D. Humphrey, Biomechanical roles of medial pooling of glycosaminoglycans in thoracic aortic dissection. *Biomech. Model. Mechanobiol.* **13**, 13–25 (2014).
35. H. Ahmadzadeh, M. K. Rausch, J. D. Humphrey, Particle-based computational modelling of arterial disease. *J. R. Soc. Interface* **15**, 20180616 (2018).
36. C. Helfenstein-Didier, D. Taïnoff, J. Viville, J. Adrien, É. Maire, P. Badel, Tensile rupture of medial arterial tissue studied by x-ray micro-tomography on stained samples. *J. Mech. Behav. Biomed. Mater.* **78**, 362–368 (2018).
37. J. M. Mattson, R. Turcotte, Y. Zhang, Glycosaminoglycans contribute to extracellular matrix fiber recruitment and arterial wall mechanics. *Biomech. Model. Mechanobiol.* **16**, 213–225 (2017).
38. Y. Zou, Y. Zhang, An experimental and theoretical study on the anisotropy of elastin network. *Ann. Biomed. Eng.* **37**, 1572–1583 (2009).
39. C. van Baardwijk, M. R. Roach, Factors in the propagation of aortic dissections in canine thoracic aortas. *J. Biomech.* **20**, 67–73 (1987).
40. X. Yu, Y. Wang, Y. Zhang, Transmural variation in elastin fiber orientation distribution in the arterial wall. *J. Mech. Behav. Biomed. Mater.* **77**, 745–753 (2018).
41. E. U. Azeloglu, M. B. Albro, V. A. Thimmappa, G. A. Ateshian, K. D. Costa, Heterogeneous transmural proteoglycan distribution provides a mechanism for regulating residual stresses in the aorta. *Am. J. Physiol. Hear Circ. Physiol.* **294**, H1197–H1205 (2008).
42. M. K. O'Connell, S. Murthy, S. Phan, C. Xu, J. Buchanan, R. Spilker, R. L. Dalman, C. K. Zarins, W. Denk, C. A. Taylor, The three-dimensional micro- and nanostructure of the aortic medial lamellar unit measured using 3D confocal and electron microscopy imaging. *Matrix Biol.* **27**, 171–181 (2008).
43. M. F. Hadi, E. A. Sander, V. H. Barocas, Multiscale model predicts tissue-level failure from collagen fiber-level damage. *J. Biomech. Eng.* **134**, 091005 (2012).
44. S. B. Shah, C. Witzenburg, M. F. Hadi, H. P. Wagner, J. M. Goodrich, P. W. Alford, V. H. Barocas, Prefailure and failure mechanics of the porcine ascending thoracic aorta: Experiments and a multiscale model. *J. Biomech. Eng.* **136**, 021028 (2014).

Acknowledgments
Funding: We would like to acknowledge the funding supports from NIH (R01 HL098028 to Y.Z. and U01 HL139466 to B.S.) and NSF (CMMI 1463390 to Y.Z.). **Author contributions:** X.Y. performed the experiments and modeling. X.Y., B.S., and Y.Z. designed the research, analyzed the data, and wrote and edited the manuscript. **Competing interests:** All authors declare that they have no competing interests. **Data and materials availability:** All data needed to evaluate the conclusions in the paper are present in the paper and/or the Supplementary Materials. Additional data related to this paper may be requested from the authors.

Submitted 14 August 2019
Accepted 18 March 2020
Published 22 May 2020
10.1126/sciadv.aaz1173

Citation: X. Yu, B. Suki, Y. Zhang, Avalanches and power law behavior in aortic dissection propagation. *Sci. Adv.* **6**, eaaz1173 (2020).